Experimental realization of spin-tensor momentum coupling in ultracold Fermi gases

Donghao Li,[1,2] Lianghui Huang,[1,2,*] Peng Peng,[1,2] Guoqi Bian,[1,2] Pengjun Wang,[1,2] Zengming Meng,[1,2] Liangchao Chen,[1,2] and Jing Zhang[1,†]

[1]*State Key Laboratory of Quantum Optics and Quantum Optics Devices, Institute of Opto-electronics, Shanxi University, Taiyuan, Shanxi 030006, People's Republic of China*

[2]*Collaborative Innovation Center of Extreme Optics, Shanxi University, Taiyuan, Shanxi 030006, People's Republic of China*

(Received 22 January 2020; revised 24 May 2020; accepted 22 June 2020; published 10 July 2020)

We experimentally realize spin-tensor momentum coupling (STMC) using three ground Zeeman states coupled by three Raman laser beams in an ultracold atomic system of ^{40}K Fermi atoms. This type of STMC consists of two bright-state bands as a spin-orbit coupled spin-1/2 system and one dark-state middle band. Using radio-frequency spin-injection spectroscopy, we investigate the energy band of STMC. It is demonstrated that the middle state is a dark state in the STMC system. The experimental realization of STMC open the door for further exploring exotic quantum matter.

DOI: 10.1103/PhysRevA.102.013309

Ultracold atomic gases provide a versatile platform for exploring many interesting quantum phenomena [1–4], which give insights into systems that are difficult to realize in solid-state systems [5–7], and especially study quantum matter in the presence of a variety of gauge fields [8–13]. A prominent example is the spin-orbit coupling (SOC), which is responsible for fascinating phenomena, such as topological insulators and superconductors [6,7], quantum spin Hall effect [14]. The synthetic one-dimensional (1D) SOC generated by a Raman transition has been implemented experimentally for bosonic [15] and fermionic [16,17] atoms. The 1D SOC has also been realized with lanthanide and alkali-metal-earth atoms [18–20]. Recently, the experimental realizations of two-dimensional SOC have been, respectively, reported in ultracold Fermi gases of ^{40}K [21,22] using a tripod scheme in a continuum space and Bose-Einstein condensate (BEC) of ^{87}Rb [23] using a scheme called an optical Raman lattice in a two-dimensional Brillouin zone where the Dirac point and nontrivial band topology are observed. All of these proposed and realized various types focus on spin-vector momentum coupling for both spin 1/2 and 1 [15–17,21–27], whereas high-order spin tensors naturally exist in a high-spin (larger or equal to 1) system.

A theoretical scheme for realizing spin-tensor momentum coupling (STMC) of spin-1 atoms has been proposed recently, and some interesting phenomena were predicted [28]. Here, STMC consists of two bright-state bands as a spin-orbit coupled spin-1/2 system and one dark-state middle band. The middle-band minimum is close to that of two bright states, so significantly modifies density of states in the ground state. This effect combining with interaction can offer a possible way to generate a new type of dynamical stripe states [28] so can bring the advantage of high visibility and long tunable periods for the direct experimental observation. Furthermore, the more complex spin-tensor momentum coupling [29] can lead to different types of triply degenerate points connected by intriguing Fermi arcs at surfaces. The STMC changes the band structure and leads to interesting many-body physics in the presence of interactions between atoms. In this paper, we experimentally realize this type of STMC with two bright-state bands and one dark-state middle band in spin-1 ultracold Fermi gases based on the scheme in Ref. [28].

Dark states in quantum optics [30] and atom optics [31] are well studied and have led to electromagnetically induced transparency [32,33], stimulated Raman adiabatic passage [34], and subrecoil cooling schemes, such as velocity selective coherent population trapping [35]. Dark states are superpositions of internal atomic ground states which are decoupled from coupling and have no energy shifts induced by coupling. In contrast, bright states have energy shifts depending on coupling strength. For example, considering Λ atomic systems (two ground states and one excited state) coupled with a pair of near-resonant fields, the excitation amplitudes of different ground states to the same excited state destructively interfere to generate a dark state. Thus, when an atom is populated in such a dark state, it remains unexcited and cannot fluoresce. In this paper, we study STMC with the bright and dark states in a Cartesian space (compared with the Brillouin zone in an optical lattice).

The realization of STMC in ultracold Fermi gases of ^{40}K atoms is illustrated in Fig. 1(a), which is similar with the scheme [28]. We choose three ground hyperfine states of ^{40}K $|\uparrow\rangle = |F = 9/2, m_F = 1/2\rangle$ ($|9/2, 1/2\rangle$), $|0\rangle = |9/2, -1/2\rangle$, and $|\downarrow\rangle = |9/2, -3/2\rangle$ of the $F = 9/2$ hyperfine level as the three internal spin states, where F denotes the total spin and m_F is the magnetic quantum number. The three spin states are coupled by three Raman laser beams to generate STMC as shown in Figs. 1(a) and 1(b). Here, two of the laser beams 1, 3 and the third laser 2 oppositely propagate along the $\hat{x}$ direction. Therefore, the three lasers beam induce two Raman transitions between the hyperfine

*Corresponding author: huanglh06@126.com
†Corresponding author: jzhang74@yahoo.com; jzhang74@sxu.edu.cn

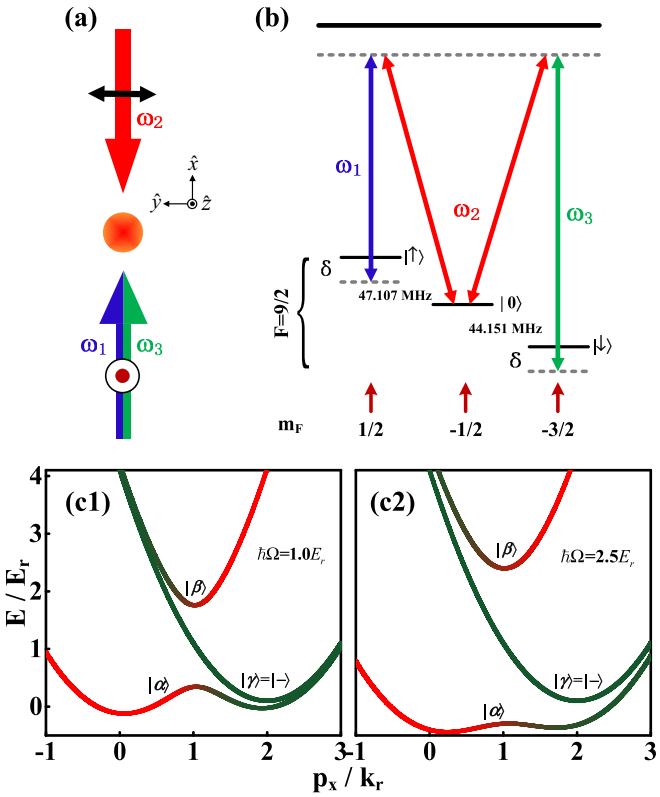

FIG. 1. Schematics of the Raman lasers configuration and atomic levels of generating STMC. (a) Raman lasers configuration to generate STMC in ultracold Fermi gases. (b) Raman transitions among three hyperfine spin states with detuning δ. (c1) and (c2) Theoretical single-particle band structure for Raman strength $\hbar\Omega_R$=1.0E_r and 2.5E_r, respectively. The detuning $\hbar\delta$ is set as 0.1E_r. The lowest band indicates eigenstate $|\alpha\rangle$, the highest band indicates eigenstate $|\beta\rangle$, and the middle one indicates eigenstate $|\gamma\rangle$.

spin-states $|0\rangle$ to the $|\uparrow(\downarrow)\rangle$ state with coupling strength Ω_{ij}, both of which have the same recoil momentum $2\hbar k_r$ along the $\hat{x}$ direction. Two Raman couplings flip atoms from $|0\rangle$ to $|\uparrow(\downarrow)\rangle$ spin states and simultaneously impart momentum $2\hbar k_r$ via the two-photon Raman process. However, the two spin-states $|\uparrow\rangle$ and $|\downarrow\rangle$ are not coupled via the Raman process due to $\Delta m_F > 1$ as shown in Fig. 1(b). The single-particle motion along the $\hat{x}$ direction can be expressed as the STMC Hamiltonian,

$$H = \hbar\begin{pmatrix} \frac{\hbar\mathbf{p}^2}{2m}+\delta & -\frac{\Omega_{12}}{2}e^{i2k_rx} & 0 \\ -\frac{\Omega_{12}}{2}e^{-i2k_rx} & \frac{\hbar\mathbf{p}^2}{2m} & -\frac{\Omega_{23}}{2}e^{i2k_rx} \\ 0 & -\frac{\Omega_{23}}{2}e^{-i2k_rx} & \frac{\hbar\mathbf{p}^2}{2m}+\delta \end{pmatrix}. \quad (1)$$

Here, δ is the two-photon Raman detuning, $\hbar k_r$ is the single-photon recoil momentum of the Raman lasers, Ω_{ij} is the coupling strength between states $|i\rangle$ and $|j\rangle$ [37], and $\hbar$ is Planck's constant. In order to eliminate the spatial dependence of the off-diagonal terms for Raman coupling in the original Hamiltonian, one can apply a unitary transformation,

$$U = \begin{pmatrix} e^{-i2k_rx} & 0 & 0 \\ 0 & 1 & 0 \\ 0 & 0 & e^{-i2k_rx} \end{pmatrix} \quad (2)$$

to get the effective Hamiltonian,

$$H_{\text{eff}} = \hbar\begin{pmatrix} \frac{\hbar(p_x-2k_r)^2}{2m}+\delta & -\frac{\Omega}{2} & 0 \\ -\frac{\Omega}{2} & \frac{\hbar p_x^2}{2m} & -\frac{\Omega}{2} \\ 0 & -\frac{\Omega}{2} & \frac{\hbar(p_x-2k_r)^2}{2m}+\delta \end{pmatrix}$$
$$= \frac{\hbar^2p_x^2}{2m} + \left(\delta + \frac{2\hbar^2k_r^2}{m} - \frac{2\hbar^2k_rp_x}{m}\right)F_z^2 - \frac{\Omega}{2}F_x. \quad (3)$$

Here, we set $\Omega_{12} = \Omega_{23} = \Omega$, p_x indicates the quasimomentum along the $\hat{x}$ direction. Here, a spin-1 system is spanned by nine basis operators, which include the identity operator (I), the three vector spin operators (F_x, F_y, and F_z), and the five spin quadrupole operators [36]. The operators F_x and F_z can be written in the matrix form

$$F_x = \begin{pmatrix} 0 & 1 & 0 \\ 1 & 0 & 1 \\ 0 & 1 & 0 \end{pmatrix}, \qquad F_z = \begin{pmatrix} 1 & 0 & 0 \\ 0 & 0 & 0 \\ 0 & 0 & -1 \end{pmatrix}. \quad (4)$$

The term $p_xF_z^2$ describes the one-dimensional coupling between a spin tensor and the linear momentum (i.e., the spin-tensor momentum coupling). We define the recoil momentum $\hbar k_r = 2\pi\hbar/\lambda$ and recoil energy $E_r = (\hbar k_r)^2/2m = \hbar\Omega_0 = h \times 8.45$ kHz as the natural momentum and energy units, where m is the atomic mass of ^{40}K, and $\lambda = 768.85$ nm is the wavelength of the Raman laser.

The three dressed eigenstates of Eq. (3) are expressed by the spin-1 basis ($|\uparrow\rangle$, $|0\rangle$, $|\downarrow\rangle$),

$$|\alpha\rangle = a_1|\uparrow\rangle + b_1|0\rangle + c_1|\downarrow\rangle, \quad (5)$$

$$|\beta\rangle = a_2|\uparrow\rangle + b_2|0\rangle + c_2|\downarrow\rangle, \quad (6)$$

$$|\gamma\rangle = a_3|\uparrow\rangle + b_3|0\rangle + c_3|\downarrow\rangle. \quad (7)$$

where $a_1 = c_1 = 1/\sqrt{u^2+2}$, $b_1 = -u/\sqrt{u^2+2}$, and $u = [(4p_x-\delta-4) - \sqrt{(4p_x-\delta-4)^2+2\Omega^2}]/\Omega$. $a_2 = c_2 = 1/\sqrt{v^2+2}$, $b_2 = -v/\sqrt{v^2+2}$, and $v = [(4p_x-\delta-4) + \sqrt{(4p_x-\delta-4)^2+2\Omega^2}]/\Omega$. $a_3 = -c_3 = 1/\sqrt{2}$ and $b_3 = 0$. The $|\alpha\rangle$ and $|\beta\rangle$ are the lowest- and highest-energy dressed states, respectively. $|\gamma\rangle$ is the middle-energy dressed state.

We define the spin components $|0\rangle$ and $|\pm\rangle = (1/\sqrt{2})(|\uparrow\rangle \pm |\downarrow\rangle)$. The middle-state $|\gamma\rangle$ corresponds to the spin dressed component $|-\rangle$. For a single-particle energy-band structure, the lowest and highest bands of STMC are the bright dressed states, which are composed of three spin components $|0\rangle$, $|\uparrow\rangle$, and $|\downarrow\rangle$ and the amplitude of three spin components depend on Ω and δ. The energy shift of the lowest and highest bands of STMC depends on the coupling strength as shown in Figs. 1(c1) and 1(c2). The highest band of STMC moves to higher energy and the lowest band to lower energy as the coupling strength increases and the detuning δ is fixed. The lowest and highest bands behave as a spin-orbit coupled spin-1/2 system. However, middle-state ($|\gamma\rangle$) is independent of Ω and δ from Eq. (7). The important point is that there is no energy shift. That is a consequence of not coupling to the Raman beams, i.e., being a dark state. The dark-state band plays an important role on both ground-state and dynamical properties of the interacting BECs with SOC as described in Ref. [28].

We start quantum degenerate gases of ^{40}K atoms at spin state $|9/2, 9/2\rangle$ by sympathetic evaporative cooling to 1.5 μK with ^{87}Rb atoms at spin-state $|2, 2\rangle$ in the quadrupole-Ioffe configuration trap and then transport them into the center of a glass cell in favor of optical access, which is used in previous experiments [37,38]. Subsequently, we typically get the degenerate Fermi gas of $(\sim 4 \times 10^6)$ ^{40}K atoms in the lowest hyperfine Zeeman-state $|9/2, 9/2\rangle$ by gradually decreasing the depth of the optical trap. Finally, we obtain ultracold Fermi gases with temperature around $0.3T_F$ where the Fermi temperature is defined by $T_F = \hbar\bar{\omega}(6N)^{1/3}/k_B$. Here, $\bar{\omega} = (\omega_x\omega_y\omega_z)^{1/3} \simeq 2\pi \times 80$ Hz is the geometric mean of the optical trap frequencies for ^{40}K degenerate Fermi gas in our experiment, N is the particle number of ^{40}K atoms, and k_B is Boltzmann's constant. After the evaporation, the remaining ^{87}Rb atoms are removed by shining a resonant laser beam pulse (780 nm) for 0.03 ms without heating and losing ^{40}K atoms. Afterwards, the atoms are transferred into spin-state $|9/2, 3/2\rangle$ using a rapid adiabatic passage induced by a rf field with duration of 80 ms at $B \simeq 19.6$ G where the center frequency of the rf field is 6.17 MHz and the scanning width is 0.4 MHz.

Three laser beams with wavelengths around 768.85 nm are used as the Raman lasers to generate the STMC along $\hat{x}$, which are extracted from a continuous-wave Ti:sapphire single frequency laser. The Raman beams 1 and 2 are frequency shifted around 74.896 and 122 MHz by two single pass acousto-optic modulators (AOMs), respectively. Raman beam 3 is double pass frequency shifted around 166.15 MHz by the AOM. Afterwards, the Raman beams 1 and 3 are coupled with the same polarization into one polarization maintaining single-mode fibers, and Raman beam 2 is sent to the second single-mode fiber to increase the stability of the beam pointing and the quality of the beam profile. Two Raman lasers 1 and 3 from the first fiber and Raman laser 2 from second fiber counterpropagate along the $\hat{x}$ axis and are focused at the position of the atomic cloud with $1/e^2$ radii of 200 μm, larger than the Fermi radius 43 μm of the degenerate Fermi gas [39] as shown in Fig. 1(a). The quantization axis is along $\hat{z}$. The two Raman laser beams 1 and 3 and Raman laser beam 2 are linearly polarized along the $\hat{z}$ and $\hat{y}$ directions, respectively, corresponding to driving π and σ transitions, respectively, shown in Fig. 1(a).

A homogeneous magnetic bias field $B_{\rm exp}$ is applied in the $\hat{z}$ axis (gravity direction) by a pair of quadrupole coils described in Ref. [21], which generates Zeeman splitting on the ground hyperfine state. We ramp the magnetic field to an expected field $B_{\rm exp} = 160$ G over 30 ms and increase the intensity of the three Raman laser beams to the desired value in 20 ms to generate STMC in three sublevels $|9/2, 1/2\rangle$, $|9/2, -1/2\rangle$, and $|9/2, -3/2\rangle$ of ultracold Fermi gases. Here, we employ spin-injection spectroscopy to measure the spin-resolved band structure. So, we prepare the other state $|9/2, 3/2\rangle$ as the initial state and use STMC as the final empty state. A Gaussian shape pulse of the rf field is applied for 450 μs to drive atoms from $|9/2, 3/2\rangle$ to the final empty state with STMC [16,17,21]. Following the spin-injection process, the Raman lasers, the optical trap, and the magnetic field are switched off abruptly, and a magnetic-field gradient is applied in the first 10 ms during the first free expansion, which creates a spatial separation of different Zeeman states due to the Stern-Gerlach effect. At last, the atoms are imaged along the $\hat{z}$ direction after total 12 ms free expansion, which gives the momentum distribution for each spin component. By counting the number of atoms in the expected state as a function of the momentum and rf frequency from the absorption image, the energy-band structure can be obtained.

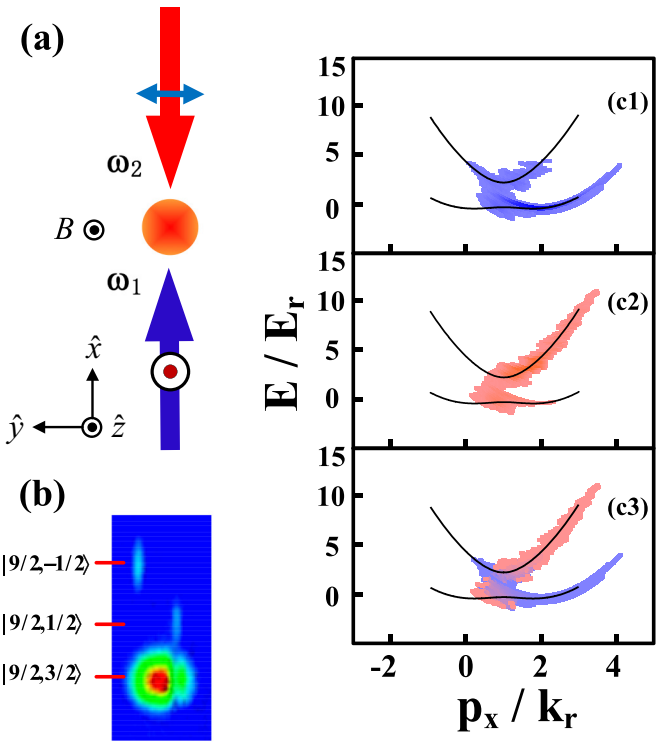

FIG. 2. Energy-band structure of 1D SOC ultracold Fermi gases. (a) A pair of Raman beams couple two spin-states $|9/2, 1/2\rangle$ ($|\uparrow\rangle$) and $|9/2, -1/2\rangle$ ($|0\rangle$) to generate the 1D SOC system with the Raman coupling strength $\hbar\Omega_R = 2.5E_r$ and the detuning $\hbar\delta = 0E_r$. (b) Time-of-flight (TOF) absorption image of spin-injection spectroscopy at a given frequency of rf field. (c1) and (c2) Reconstructed momentum- and spin-resolved $|\uparrow\rangle$ (blue) and $|0\rangle$ (red) spectra, respectively, when driving atoms from the free spin-state $|9/2, 3/2\rangle$. (c3) Displaying two graphs (c1) and (c2) simultaneously.

First, we measure energy-band structure of standard 1D SOC as shown in Fig. 2 which is similar as that reported in Ref. [17]. We prepare the atoms in the free spin-state $|3/2, 9/2\rangle$, then, switch on two Raman lasers to generate the 1D SOC system with two spin-states $|\uparrow\rangle$ and $|0\rangle$. Using rf spin injection, we get the energy-band structure of 1D SOC, which agrees with the theoretical calculation well as shown in Fig. 2(c).

Now, we study STMC and illustrate the middle-state $|\gamma\rangle$ as a dark state in the STMC system. We prepare the ultracold atomic sample in the free-state $|9/2, 3/2\rangle$ with a fixed magnetic field, then, switch on three Raman laser to generate the STMC system. Afterwards, we use rf spin injection from the free state to empty the STMC system as shown in Fig. 3(a).

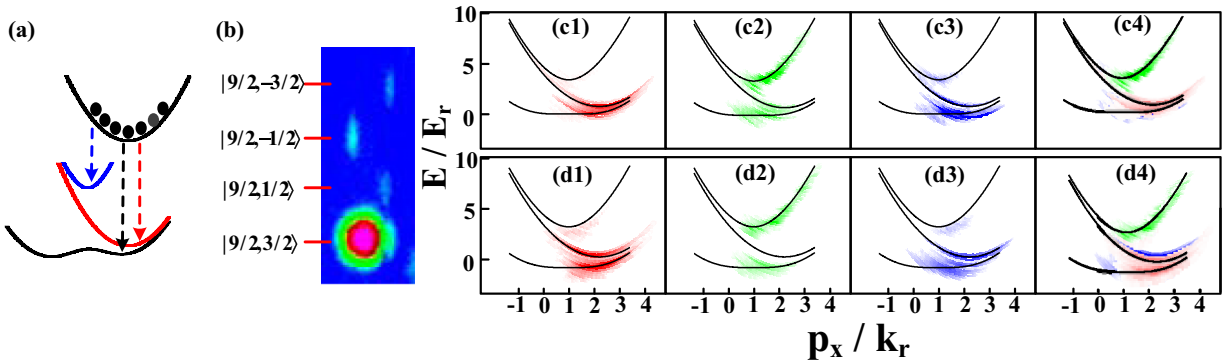

FIG. 3. Energy-band structure of STMC ultracold Fermi gases. (a) Schematic of the process of spin-injection spectroscopy with preparing in the free spin-state $|9/2, 3/2\rangle$. The vertical arrows represent the transitions driven by the rf field. The frequency of the rf field is scanned. (b) TOF image of spin-injection spectroscopy at a given frequency of the rf field. (c1)–(c3) Reconstructed spin-resolved $|\uparrow\rangle$ (red), $|0\rangle$ (green), and $|\downarrow\rangle$ (blue) spectra, respectively, when driving atoms from the free spin-state $|9/2, 3/2\rangle$ to the STMC system with the Raman coupling strength $\hbar\Omega = 2.5E_r$ and the detuning $\hbar\delta = 0E_r$. (c4) Displaying the three graphs (c1)–(c3) simultaneously. (d1)–(d4) spin-injection spectroscopy with the values of $\hbar\Omega = 3E_r$ and $\hbar\delta = 0E_r$.

We obtain the energy spectrum of the STMC system as shown in Fig. 3. Here, the detuning $\delta = 0$, and the Raman coupling strength $\Omega = 2.5\Omega_0$ ($3\Omega_0$) shown in Figs. 3(c) and 3(d).

The three spin components appear in TOF images [for example, in Fig. 3(b)] simultaneously when the rf field drives atoms into the lowest and highest bands. The color depth contains the amplitude information of three spin components for the lowest and highest bands in Figs. 3(c) and 3(d). The highest band of STMC moving to higher energy and the lowest band to lower energy as the coupling strength increases are shown in Figs. 3(c) and 3(d). It illustrates that the lowest and highest bands are the bright dressed states and behave as a spin-orbit coupled spin-1/2 system. However, the middle dressed-state $|\gamma\rangle$ only includes two spin components $|\uparrow\rangle$ and $|\downarrow\rangle$ (the spin dressed-state $|-\rangle$). Therefore, we only observe the two spin components $|\uparrow\rangle$ and $|\downarrow\rangle$ in the middle band from the rf spectrum. Especially, almost no atoms in the $|0\rangle$ spin component are populated in the middle band as shown in Figs. 3(c2) and 3(d2). Moreover, Figs. 3(c) and 3(d) show that the middle-state $|\gamma\rangle$ is always a dark state without energy shift and decouples from the Raman strength Ω.

We also employ another rf spectrum method to measure the energy-band structure of the STMC state [16]. Here, atoms are prepared in STMC as the initial state, and state $|9/2, 3/2\rangle$ is used as the final empty state. We first prepare the ultracold atomic sample in state $|9/2, 1/2\rangle$ at first, then ramp on three Raman lasers with 5 ms to prepare Fermi atoms into the STMC state in equilibrium. Then, we apply the rf pulse to drive the atoms from the STMC state into free-state $|9/2, 3/2\rangle$ as shown in Fig. 4(a). We also get the energy spectrum of the STMC system as shown in Figs. 4(b) and 4(c). Here, the Raman coupling strength is $\Omega = 2.5\Omega_0$ and the detuning $\delta = 0$. For the rf spectrum of STMC, the populated range into three bands of STMC is determined by the temperature of Fermi gases. The higher temperatures of the Fermi gases will make the momentum distribution broader, which will enlarge the measure range of the energy band with compromising the signal-to-noise ratio of the rf spectroscopy.

In conclusion, we have realized a scheme for generating the STMC system in ultracold Fermi gases and demonstrate coupling between the internal state of the atoms and their momenta in a multilevel system. We measure and get the energy-band structure of STMC via the rf spin-injection spectrum. From the rf spin-injection spectrum, we demonstrated that the middle-state $|\gamma\rangle$ in the STMC system is a dark state. In this paper, the dark-state band is not coupled with two bright-state bands through Raman coupling only for the single-particle picture. Since the dark-state band is a dressed and excited state, atoms will decay into the ground bright band due to interaction if we prepare atoms initially in the dark-state band. Moreover, forming the dark-state band requires that the Raman detuning δ for $|\uparrow\rangle$ and $|\downarrow\rangle$ are exactly same. Otherwise, the dark-state band will change into the bright band. The experimental results may motivate more theoretical and experimental research of many interesting quantum phases and multicritical points for phase transitions, such as study the supersolidlike stripe order due to the existence of the dark middle band and may give rise to nontrivial topological

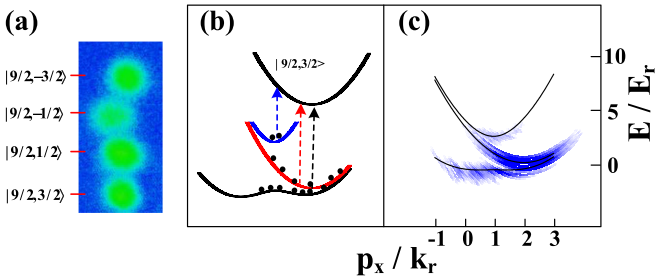

FIG. 4. Another method to measuring momentum-resolved rf spectroscopy of the STMC ultracold Fermi gases. (a) Time-of-flight absorption image of rf spectroscopy at a given frequency of the rf field. (b) Schematic of the process of rf spectroscopy with initially preparing atoms in STMC. The vertical arrows represent the transitions driven by the rf field. (c) Reconstructed single-particle dispersion and atom population when transferring atoms from the STMC ultracold Fermi gases system to free spin-state $|9/2, 3/2\rangle$ for $\hbar\Omega = 2.5E_R$ and the detuning $\hbar\delta = 0E_R$.

matter (STMC in optical lattices where nontrivial topological bands may emerge).

We would like to thank C. Zhang for helpful discussions. This research was supported by the MOST (Grants No. 2016YFA0301602 and No. 2018YFA0307601), NSFC (Grants No. 11974224, No. 11704234, No. 11804203, and No. 11904217), the Fund for Shanxi "1331 Project" Key Subjects Construction, and the Program of Youth Sanjin Scholar.

[1] I. Bloch, J. Dalibard, and W. Zwerger, Many-body physics with ultracold gases, Rev. Mod. Phys. **80**, 885 (2008).
[2] C. Chin, R. Grimm, P. Julienne, and E. Tiesinga, Feshbach resonances in ultracold gases, Rev. Mod. Phys. **82**, 1225 (2010).
[3] D. M. Stamper-Kurn and M. Ueda, Spinor Bose gases: Symmetries, magnetism, and quantum dynamics, Rev. Mod. Phys. **85**, 1191 (2013).
[4] F. Dalfovo, S. Giorgini, L. P. Pitaevskii, and S. Stringari, Theory of Bose-Einstein condensation in trapped gases, Rev. Mod. Phys. **71**, 463 (1999).
[5] D. Xiao, M. C. Chang, and Q. Niu, Berry phase effects on electronic properties, Rev. Mod. Phys. **82**, 1959 (2010).
[6] M. Z. Hasan and C. L. Kane, *Colloquium:* Topological insulators, Rev. Mod. Phys. **82**, 3045 (2010).
[7] X.-L. Qi and S.-C. Zhang, Topological insulators and superconductors, Rev. Mod. Phys. **83**, 1057 (2011).
[8] J. Dalibard, F. Gerbier, G. Juzeliunas, and P. Ohberg, Colloquium: Artificial gauge potentials for neutral atoms, Rev. Mod. Phys. **83**, 1523 (2011).
[9] V. Galitski and I. B. Spielman, Spin-orbit coupling in quantum gases, Nature (London) **494**, 49 (2013).
[10] N. Goldman, G. Juzeliunas, P. Ohberg, and I. B. Spielman, Light-induced gauge fields for ultracold atoms, Rep. Prog. Phys. **77**, 126401 (2014).
[11] H. Zhai, Degenerate quantum gases with spin-orbit coupling: a review, Rep. Prog. Phys. **78**, 026001 (2015).
[12] J. Zhang, H. Hu, X.-J. Liu, and H. Pu, Fermi gases with synthetic spin-orbit coupling, Annu. Rev. Cold At. Mol. **2**, 81 (2014).
[13] D.-W. Zhang, Y.-Q. Zhu, Y. X. Zhao, H. Yan, and S.-L. Zhu, Topological quantum matter with cold atoms, Adv. Phys. **67**, 253 (2018).
[14] S. R. Elliott and M. Franz, *Colloquium:* Majorana fermions in nuclear, particle, and solid-state physics, Rev. Mod. Phys. **87**, 137 (2015).
[15] Y.-J. Lin, K. J. Garcia, and I. B. Spielman, Spin–orbit-coupled Bose–Einstein condensates, Nature (London) **471**, 83 (2011).
[16] P. Wang, Z. Yu, Z. Fu, J. Miao, H. Huang, J. Chai, H. Zhai, and J. Zhang, Spin-Orbit Coupled Degenerate Fermi Gases, Phys. Rev. Lett. **109**, 095301 (2012).
[17] L. W. Cheuk, A. T. Sommer, Z. Hadzibabic, T. Yefsah, W. S. Bakr, and M. W. Zwierlein, Spin-Injection Spectroscopy of a Spin-Orbit Coupled Fermi Gas, Phys. Rev. Lett. **109**, 095302 (2012).
[18] N. Q. Burdick, Y. Tang, and B. L. Lev, Long-Lived Spin-Orbit-Coupled Degenerate Dipolar Fermi Gas, Phys. Rev. X **6**, 031022 (2016).
[19] L. F. Livi, G. Cappellini, M. Diem, L. Franchi, C. Clivati, M. Frittelli, F. Levi, D. Calonico, J. Catani, M. Inguscio, and L. Fallani, Synthetic Dimensions and Spin-Orbit Coupling with an Optical Clock Transition, Phys. Rev. Lett. **117**, 220401 (2016).
[20] S. Kolkowitz, S. L. Bromley, T. Bothwell, M. L. Wall, G. E. Marti, A. P. Koller, X. Zhang, A. M. Rey, and J. Ye, Spin-orbit-coupled Fermions in an optical lattice clock, Nature (London) **542**, 66 (2017).
[21] L. Huang, Z. Meng, P. Wang, P. Peng, S. Zhang, L. Chen, D. Li, Q. Zhou, and J. Zhang, Experimental realization of two-dimensional synthetic spin-orbit coupling in ultracold Fermi gases, Nat. Phys. **12**, 540 (2016).
[22] Z. Meng, L. Huang, P. Peng, D. Li, L. Chen, Y. Xu, C. Zhang, P. Wang, and J. Zhang, Experimental Observation of a Topological Band Gap Opening in Ultracold Fermi Gases with Two-Dimensional Spin-Orbit Coupling, Phys. Rev. Lett. **117**, 235304 (2016).
[23] Z. Wu, L. Zhang, W. Sun, X. Xu, B. Wang, S. Ji, Y.-J. Deng, S. Chen, X.-J. Liu, and J.-W. Pan, Realization of two-dimensional spin-orbit coupling for Bose-Einstein condensates, Science **354**, 83 (2016).
[24] Z. Fu, P. Wang, S. Chai, L. Huang, and J. Zhang, Bose-Einstein condensate in a light-induced vector gauge potential using the 1064 nm optical dipole trap lasers, Phys. Rev. A **84**, 043609 (2011).
[25] J.-Y. Zhang, S.-C. Ji, Z. Chen, L. Zhang, Z.-D. Du, B. Yan, G.-S. Pan, B. Zhao, Y.-J. Deng, H. Zhai, S. Chen, and J.-W. Pan, Collective Dipole Oscillations of a Spinorbit Coupled Bose-Einstein Condensate, Phys. Rev. Lett. **109**, 115301 (2012).
[26] C. Qu, C. Hamner, M. Gong, C. Zhang, and P. Engels, Observation of zitterbewegung in a spin-orbit-coupled Bose-Einstein condensate, Phys. Rev. A **88**, 021604 (2013).
[27] A. Olson, S. Wang, R. Niffenegger, C. Li, C. Greene, and Y. Chen, Tunable Landau-Zener transitions in a spin-orbit-coupled Bose-Einstein condensate, Phys. Rev. A **90**, 013616 (2014).
[28] X. Luo, K. Sun, and C. Zhang, Spin-Tensor-Momentum-Coupled Bose-Einstein Condensates, Phys. Rev. Lett. **119**, 193001 (2017).
[29] H. Hu, J. Hou, F. Zhang, and C. Zhang, Topological Triply Degenerate Points Induced by Spin-Tensor-Momentum Couplings, Phys. Rev. Lett. **120**, 240401 (2018).
[30] M. O. Scully and M. S. Zubairy, *Quantum Optics* (Cambridge University Press, 1997).
[31] E. Arimondo, Coherent population trapping in laser spectroscopy, Prog. Opt. **35**, 259 (1996).
[32] K. J. Boller, A. Imamoğlu, and S. E. Harris, Observation of Electromagnetically Induced Transparency, Phys. Rev. Lett. **66**, 2593 (1991).
[33] M. Fleischhauer, A. Imamoğlu, and J. Marangos, Electromagnetically induced transparency: Optics in coherent media, Rev. Mod. Phys. **77**, 633 (2005).
[34] J. R. Kuklinski, U. Gaubatz, T. F. Hioe, and K. Bergmann, Adiabatic population transfer in a three-level system driven by delayed laser pulses, Phys. Rev. A **40**, 6741 (1989).

[35] A. Aspect, E. Arimondo, R. Kaiser, N. Vansteenkiste, and C. Cohen-Tannoudji, Laser Cooling below the One-Photon Recoil Energy by Velocity-Selective Coherent Population Trapping, Phys. Rev. Lett. **61**, 826 (1988).

[36] G. E. Marti and D. M. Stamper-Kurn, Spinor Bose-Einstein gases, in *Quantum Matter at Ultralow Temperatures*, Proceedings of the International School of Physics "Enrico Fermi", edited by M. Inguscio, W. Ketterle, S. Stringari, and G. Roati (IOS, Amsterdam, 2016), pp. 221–291.

[37] L. Huang, P. Wang, Z. Meng, P. Peng, L. Chen, D. Li, and J. Zhang, Magnetic-field dependence of Raman coupling strength in ultracold ^{40}K atomic Fermi gas, Chin. Phys. Lett. **33**, 033401 (2016).

[38] S. Chai, P. Wang, Z. Fu, L. Huang, and J. Zhang, The design of a dipole traps for Bose-Einstein condensate and degenerate Fermi gas, Acta Sinica Quantum Optica **18**, 171 (2012).

[39] S. Giorgini, L. P. Pitaevskii, and S. Stringari, Theory of ultracold atomic Fermi gases, Rev. Mod. Phys. **80**, 1215 (2008).